Nano Research

ISSN 1998-0124 CN 11-5974/O4
https://doi.org/10.1007/s12274-019-2443-3

Research Article

All-in-one cellulose based hybrid tribo/piezoelectric nanogenerator

Ming Li[1,2,§], Yang Jie[1,2,§], Li-Hua Shao[3,§], Yilin Guo[1,2], Xia Cao[1,2,4] (✉), Ning Wang[4] (✉), and Zhong Lin Wang[1,2,5] (✉)

[1] *Beijing Institute of Nanoenergy and Nanosystems, Chinese Academy of Sciences, National Center for Nanoscience and Technology (NCNST), Beijing 100083, China*
[2] *School of Nanoscience and Technology, University of Chinese Academy of Sciences, Beijing 100049, China*
[3] *Institute of Solid Mechanics, Beihang University, Beijing 100083, China*
[4] *Research Center for Bioengineering and Sensing Technology, Beijing Key Laboratory for Bioengineering and Sensing Technology, School of Chemistry and Biological Engineering, Beijing Municipal Key Laboratory of New Energy Materials and Technologies, and Center for Green Innovation, School of Mathematics and Physics, University of Science and Technology Beijing, Beijing 100083, China*
[5] *School of Materials Science and Engineering, Georgia Institute of Technology, Atlanta, Georgia 30332, USA*
[§] *Ming Li, Yang Jie, and Li-Hua Shao contributed equally to this work.*

Received: 11 March 2019 / **Revised:** 28 April 2019 / **Accepted:** 20 May 2019

ABSTRACT

Aybrid tribo/piezoelectric nanogenerators (HTPENG) have been proven to be highly efficient and versatile as far as the collection and conversion of ambient energy are concerned, and the introduction of flexible and green materials is a key step for their potential applications. Here, we developed a HTPENG by using nitrocellulose nanofibril paper as the triboelectric layer and $BaTiO_3$/MWCNT@bacterial cellulose paper as the piezoelectric layer. The output of the triboelelctric paper has considerable performance as fluorinated ethylene propylene, and the output of piezoelectric paper is more than ten times higher than the BTO/polydimethylsiloxane structure. The integrated outputs of the sandwich structured HTPENG are 18 V and 1.6 μA·cm^{-2}, which are capable of lighting up three LED bulbs and charging a 1 μF capacitor to 2.5 V in 80 s. In addition, the voltage signal generated by the HTPENG in contact-separation mode can be used for dynamic pressure detection. The linear range of dynamic pressure is from 0.5 to 3 N·cm^{-2} with a high sensitivity of 8.276 V·cm^2·N^{-1} and a detection limit of 0.2 N·cm^{-2}. This work provides new insights into the design and application of cellulose-based hybrid nanogenerators with high flexibility and simple structure.

KEYWORDS

cellulose, hybrid nanogenerator, energy harvesting, pressure sensor

1 Introduction

With the growing energy crisis and environmental concerns, the hybrid tribo/piezoelectric nanogenerator (HTPENG) is attracting intensive attention because they can harvest various kinds of ambient energy such as body movements [1], air flow [2], acoustic wave [3], and water wave [4] via the piezoelectric [5, 6] and triboelectric [7] effects. In general, triboelectric nanogenerator (TENG) consists of two materials with different electron affinity and takes advantage of the coupled triboelectrification effect and electrostatic induction [8]. The triboelectrically positive materials used in TENG include polyamides [9], metals [10], indium tin oxide (ITO) [11] and zinc oxide (ZnO) [12], while the negative materials include the fluorinated ethylene propylene (FEP) [13], polytetrafluoroethylene (PTFE) [14] polyvinylidene fluoride (PVDF) [2], polydimethylsiloxane (PDMS) [15], and polyethylene terephthalate (PET) [16]. Meanwhile, piezoelectric materials such as ZnO nanowires [5], GaN [17], PVDF [18], $BaTiO_3$ (BTO) nanoparticles [19] have been widely studied for the design of piezoelectric nanogenerator (PENG), which can convert piezoelectric energy into electricity due to the piezoelectric effects [20–23]. However, the hybridization of these nanogenerators involves complicated manufacturing process, and the limited output power and poor biocompatibility are the main constraints for their practical applications.

As the most abundant natural polymer on earth, cellulose provides a sustainable green resource that is renewable, degradable, and biocompatible. A large number of hydrogen bonds existed within and between the molecules produce not only different configurations of cellulose structures but also offer a unique combination of various properties including flexible surface, transparency, low thermal expansion, high elasticity and anisotropy [24–26]. Up to now, various energy-converting devices have been made from cellulose, including solar energy collection [27], mechanical energy collection [28] and energy storage [29]. On the one hand, cellulose can serve as a matrix for functional materials like flexible transparent films and conductive polymers. On the other hand, the introduction of cellulose into HTPENG may endow them the property of natural degradation, recyclability, and biocompatibility.

Thus in this work, we present a HTPENG by combing the triboelectric paper based on cellulose nanofibril (CNF) and piezoelectric paper based on bacterial cellulose (BC). The CNF fibers were further treated with a mixed solution of HNO_3 and H_2SO_4. After the functionalization, the $-NO_3$ group is introduced to increase the tendency to gain the electrons (electronegativity). The piezoelectric paper was made from BC and BTO nanoparticles through a vacuum filtration method. Meanwhile, multi-walled carbon nanotubes (MWCNTs) was dispersed into the piezoelectric paper to achieve a unique entangled network structure, which can reduce the internal

Address correspondence to Xia Cao, caoxia@binn.cas.cn; Ning Wang, wangning@ustb.edu.cn; Zhong Lin Wang, zlwang@gatech.edu

resistance and improve the piezoelectric characteristics. The TENG and PENG showed high outputs, the open-circuit voltage and short-circuit current density can reach 37 V, 1.23 μA·cm^{-2} and 22 V, 220 nA·cm^{-2}, respectively. Using a full-wave bridge diode to effectively integrate the two outputs, the HTPENG's outputs are 18 V and 1.6 μA·cm^{-2}, which is capable of lighting up three LED bulbs and charging a 1 μF capacitor to 2.5 V in 80 s. In addition, HTPENG can be used as a pressure sensor because it can produce a linearly correlated pulsed voltage signal in the contact-separation mode. The linear range of dynamic pressure is from 0.5 to 3 N·cm^{-2} with a high sensitivity of 8.276 V·cm^2·N^{-1} and a detection limit of 0.2 N·cm^{-2}. The HTPENG based on cellulose has the characteristics of light weight, environmental friendly, easy processing, and cost-effective, which can provide a choice for further implementing wearable or implantable devices, self-powered electronic devices.

2 Experimental

2.1 Fabrication of the Nitro-CNF paper

The wood cellulose nanofibers CNF are vigorously stirred and dispersed in water with sonication. At room temperature, a mixed solution of HNO_3 and H_2SO_4 is added to the CNF dispersion (the mass ratios of HNO_3 and H_2SO_4 are 40% and 60%, respectively). After 2 h of reaction, the mixture is washed with deionized water and centrifuged several times to collect Nitro-CNF aqueous suspension. Then the suspension is sonicated and vacuum filtered through a PVDF microporous membrane. At last, the filtrated film is flattened by a 2 kg weight and dried at 50 °C for 36 h to obtain the Nitro-CNF paper.

2.2 Fabrication of the functionalized BC piezoelectric paper

The BC hydrogel is vigorously stirred for 30 min so that it is uniformly dispersed in water. Hydrothermal BTO nanoparticles and MWCNT are ultrasonically dispersed in distilled water and then mixed with BC aqueous suspension. The mass ratios of BTO, MWCNT, and BC in the mixed solution are 70%, 10% and 20%, respectively. The well-mixed dispersions are vacuum filtered by a PVDF microporous membrane. Finally, the filtrated film is flattened by a 2 kg weight and dried at 60 °C for 24 h to obtain the piezoelectric paper.

2.3 Fabrication of the HTPENG

The piezoelectric paper and the triboelectric paper are cut into 1.5 cm × 1.0 cm to prepare for the production of a HTPENG. The HTPENG consists of vertically-stacked two layers. The top layer is a PENG consisting of a nickel-electrode-encapsulated BC (BTO/MWCNT) piezoelectric paper sandwich arch, and the bottom layer is a contact-separation mode TENG of the Nitro-CNF triboelectric paper structure with a nickel electrode, where the bottom electrode of the PENG serves as a shared common electrode and as a driving electrode of TENG.

2.4 Characterization

The morphology and size of the BC (BTO/MWCNT) piezoelectric papers were characterized by the field-emission scanning electron microscopy (FE-SEM, Quanta 450). The piezoelectric and triboelectric papers were applied to the nickel electrode by Denton Multi-target Magnetic Control Sputtering System (Discovery 635). The crystalline structures of BTO nanoparticles were characterized by X-ray diffractometer (Xpert3 powder). The pristine-CNF and Nitro-CNF papers were scanned from 4,000 to 500 cm^{-1} with Fourier transform infrared (FTIR, VERTEX80v) spectrophotometer in attenuated total reflectance mode (ATR). A programmable electrometer (6514 system) was used to test the electrical signals.

3 Results and discussion

Figures 1(a) and 1(b) shows the fabrication process of the Nitro-CNF triboelectric papers and functionalized BC piezoelectric papers, respectively. The raw wood CNF and BC are transparent hydrogels, which are subjected to the corresponding functionalization process to obtain the blended suspension and finally vacuum filtered to form papers. The side-view SEM image of the piezoelectric paper is shown in Fig. 1(c). The piezoelectric paper owes the rough surface at the micro-nano scale, which means the BTO nanoparticles have been uniformly distributed in the BC paper. Figure 1(d) shows the X-ray diffraction (XRD) pattern of BTO nanoparticles. Six diffraction peaks, (100), (110), (111), (200), (210), and (211) at 22.1°, 31.5°, 38.8°, 45.1°, 50.8°, and 55.9° can be observed, which represent a high piezoelectric tetragonal phase of BTO. As shown in Fig. 1(e), to further ensure the ferro-and piezo-electric properties of the BC/BTO piezoelectric paper, polarization (P)–electric field (E) hysteresis loop is measured,which shows remnant polarization (Pr) of 0.13 μC·cm^{-2} at a maximum applied electric field of 40 kV·cm^{-1}. Fourier transform infrared spectroscopy (FTIR) characterization was performed to analyze the chemical structure of the pristine-CNF and Nitro-CNF papers, as shown in Fig. 1(f). The pristine-CNF (bottom curve) shows the absorptions of C–O–C stretching within the pyranose ring skeletal (at 1,050 cm^{-1}), O–H stretching (3,500 cm^{-1}), and C–H stretching (2,900 cm^{-1}). Comparing to the pristine-CNF, the Nitro-CNF (top curve) presents three new intense peaks positioned at 1,640, 1,275, 832 cm^{-1}, which are the corresponding asymmetric and symmetric stretching of the –NO_2 group and stretching of the N–O bonds, respectively. For Nitro-CNF, the nitration process should

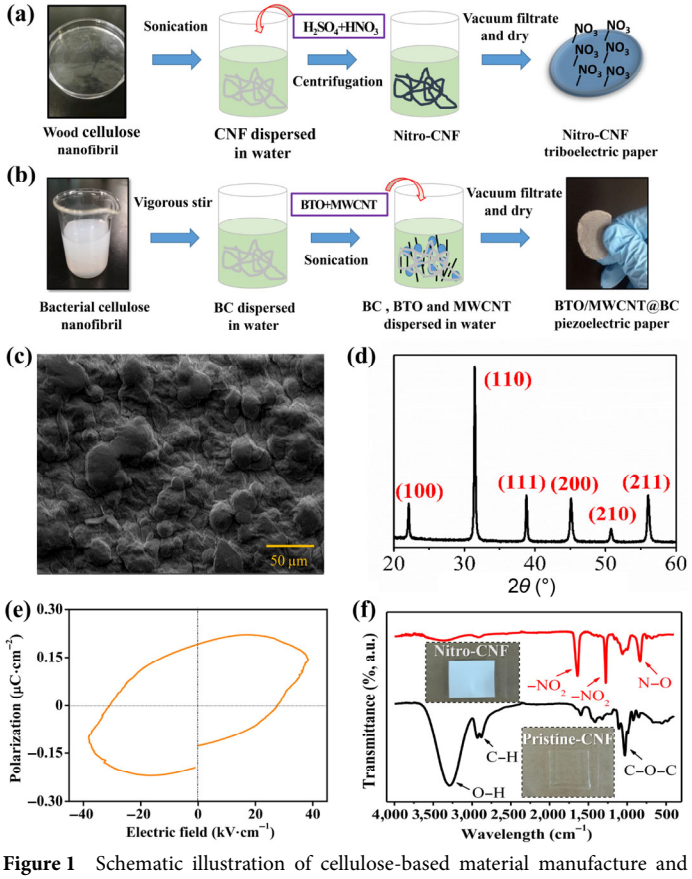

Figure 1 Schematic illustration of cellulose-based material manufacture and characterization. (a) The flow chart of the triboelectric paper preparation. (b) The flow chart of the piezoelectric paper preparation. (c) The SEM image of the piezoelectric paper. (d) The X-ray diffraction pattern of BTO nanoparticle loaded in the piezoelectric paper. (e) The P-E loop of the BC/BTO piezoelectric paper. (f) FTIR spectrum of Nitro-CNF (top) and pristine CNF (bottom). The inset pictures show the films fabricated from two kinds of cellulosic materials.

render the substitution of hydroxyl groups by nitrate ester groups. CNF is slightly tribopositive due to the intrinsic abundant oxygen atoms in cellulose and the small amount of carboxylic groups produced from the nanofibrillation processing of cellulose pulp. Nitro-CNF is tribonegative since it carries strong electron-withdrawing nitro groups [30]. Therefore we chose Nitro-CNF as the triboelectric layer.

Figure 2(a) shows the 3-D schematic image of the HTPENG, which consists of the vertically-stacked two layers: the top layer is a PENG consisting of a nickel-electrode-encapsulated functionalized BC piezoelectric paper sandwich arch, and the bottom layer is the Nitro-CNF triboelectric paper structure with a nickel electrode. The arched shape of the PENG enhances the strength of the effective strain applied in the BC layer and drives the shape of the HTPENG to an initial state when the applied force is released. In order to integrate the piezoelectric and triboelectric mechanisms simultaneously, we use the bottom electrode of the PENG as the driving electrode of the TENG. Figure 2(b) shows the photo of the HTPENG in which the triboelectric and piezoelectric paper dimensions are both 1.5 cm × 1.0 cm. Note that we did not perform further surface treatments on BC paper and Nitro-CNF paper.

Figure 2(c) shows the working mechanism of the HTPENG in a contact-separation cycle. At the initial state, neither the triboelectric nor the piezoelectric potential exists before the contact of the two layers. When an external force is applied to the top layer, the functionalized BC paper has tensile stress, and the positive piezoelectric potential is generated by the deformation between the upper and lower nickel electrodes. As shown in Fig. 2(c)-(I), the electrons flow from the lower nickel electrode to the upper nickel electrode driven by the piezoelectric potential. Once the top layer contacts the bottom layer (full contact state), the physical contact between the nickel electrode and the Nitro-CNF paper induces the charge transfer. Since the Nitro-CNF obtains electrons more easily than the nickel electrode, the electrons are transferred and held as shown in Fig. 2(c)-(II). Both of the triboelectric and piezoelectric outputs reach a maximum at the moment of full contact. When the applied force is released (separated state) as shown in Fig. 2(c)-(III), the electrons of the triboelectric layer return to nickel. Due to the compressive force of the functionalized BC (MWCNT/BTO) paper, the HTPENG produces both the negative triboelectric and the positive piezoelectric outputs, thus the electrons flow from Cu and the lower nickel electrode to the upper nickel electrode. When two layers are completely separated, the triboelectric layer has no triboelectric potential because of the electron neutralization as shown in Fig. 2(c)-(IV). Meanwhile, the functionalized BC paper produces a maximum piezoelectric output owing to the maximum strain in the initial state, and the piezoelectric charge slowly decreases. Finally, a full cycle is completed, and it will go back to the balance state. Therefore, we obtained both the triboelectric and piezoelectric output signals in a contact-separation cycle.

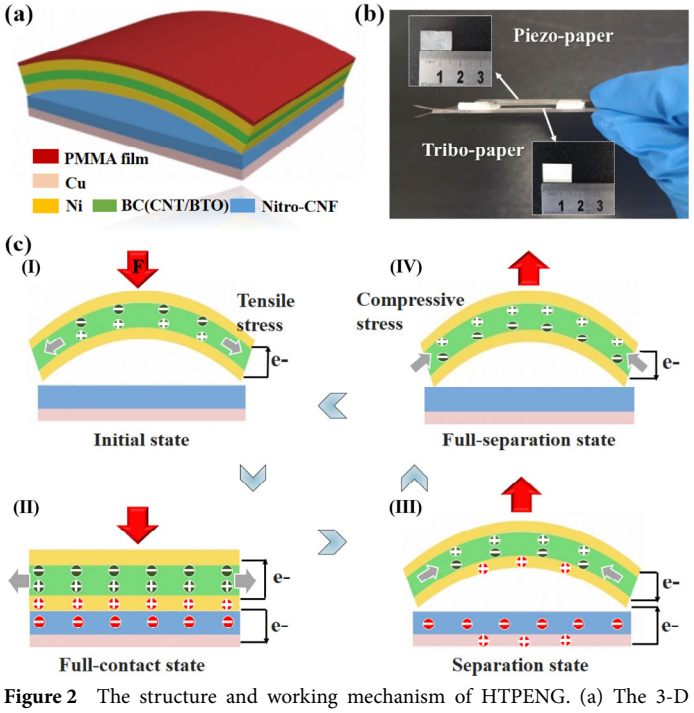

Figure 2 The structure and working mechanism of HTPENG. (a) The 3-D schematic view of the arch-shaped HTPENG. (b) The photo of the HTPENG. (c) The working mechanism of the HTPENG in a contact-separation cycle. (I) Piezoelectric effect charge distribution when the external force applied. (II) Piezoelectric and triboelectric charge distribution at full-contact state. (III) Negative PENG and TENG at separating state. (IV) The maximum negative piezoelectric potential under full- separation state.

In this experiment, the dynamic pressure was applied to the device by a shaker motor, which provides a steady, continuous, and periodically variable force. The output performance of the device was investigated by measuring the open-circuit voltage and the short-circuit current when the HTPENG was subjected to a cyclic vertical external force at the frequency of 5 Hz and the dynamic pressure of 2 N·cm^{-2}. Like the corresponding working mechanism, the short-circuit current density exhibits AC behavior, with an equal amount of electrons flowing in opposite directions within one cycle. The open-circuit voltage switched between zero and a plateau value, respectively, corresponding to the original position and the contact position. The open-circuit voltage increases until reaching the maximum peak value when a full contact is made again between the two triboelectric layers. The open-circuit voltage drops from the maximum peak value to zero when the Nitro-CNF paper fully reverts to the original position. As shown in Figs. 3(a) and 3(b), the open-circuit voltage and short-circuit current density of the triboelectric part can reach to as high as 37 V and 1.23 μA·cm^{-2}, respectively. In

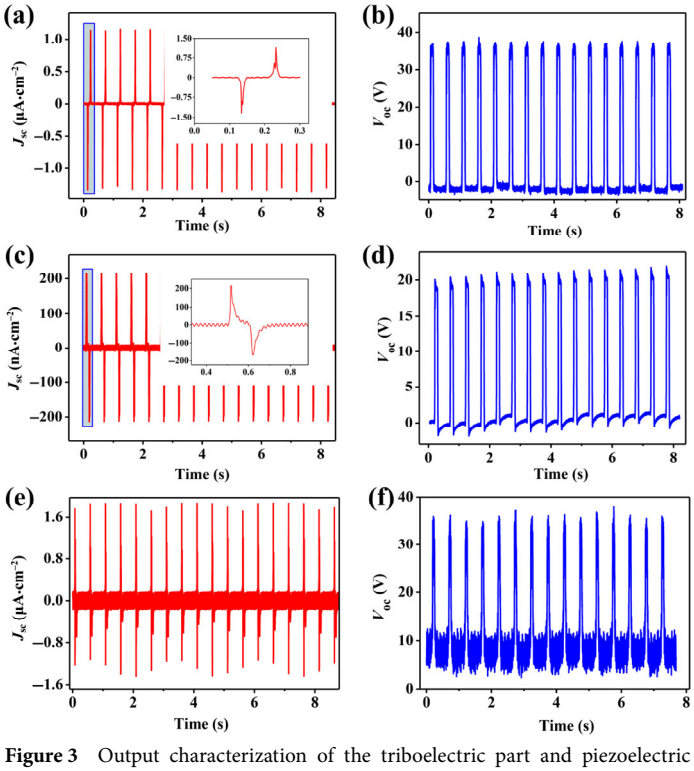

Figure 3 Output characterization of the triboelectric part and piezoelectric part. (a) The short-circuit current density of triboelectric part. The inset shows a cycle of an enlarged current curve. (b) The open-circuit voltage of triboelectric part. (c) The short-circuit current density of piezoelectric part. The inset shows a cycle of an enlarged current curve. (d) The open-circuit voltage of piezoelectric part. (e) The short-circuit current density of FEP and Ni as the triboelectric layer under the same area. (f) The open-circuit voltage of FEP and Ni as the tricoelectric layer under the same area.

addition, disordered dipoles in ferroelectric BTO domains need to be aligned by an external electric field. In order to enhance the piezoelectric potential in a specific direction to better measure the output of the piezoelectric part, electrical poling process is an indispensable step for the BTO/BC piezoelectric paper. Therefore, we detected the output signal of the BC/BTO piezoelectric paper when the poling electric field is 200 kV·cm^{-1}. Figures 3(c) and 3(d) shows the open-circuit voltage and short-circuit current density of the piezoelectric part are up to 22 V and 220 nA·cm^{-2}, respectively. It is higher than the output of the same type of BC/BTO piezoelectric paper without the added MWCNT (14 V and 190 nA·cm^{-2}) [31]. This demonstrates that the added MWCNT helps to realize the entangled network structure and enhance the piezoelectric characteristics. Comparing with the output performance of the FEP film and Ni with the same area, the output of the triboelectric part of HTPENG is still considerable, as shown in Figs. 3(e) and 3(f).

Figures 4(a) and 4(b) illustrates the dependence of the piezoelectric and triboelectric output characteristic on the external load resistance. With the increment of the load resistance from 1 MΩ to 1 GΩ, the open-circuit voltage of the piezoelectric part increases gradually from 0.15 to 20 V, and the short-circuit current density decreases from 185 to 19 nA·cm^{-2}. Simultaneously, the open-circuit voltage of the triboelectric part increases gradually from about 0.50 to 37 V, and the short-circuit current density decreases from 1.21 to 0.05 μA·cm^{-2}. As plotted in Figs. 4(d), the corresponding piezoelectric part maximum power density is 1.21 μW·cm^{-2} at a matched resistance value of 60 MΩ and the triboelectric part maximum power density is 10.6 μW·cm^{-2} at a matched resistance value of 80 MΩ, respectively.

After connecting a full-wave bridge diode to the HTPENG, the open-circuit output voltage and current density of HTPENG are 18 V and 1.6 μA·cm^{-2} as shown in Figs. 5(a) and 5(b), respectively. With the bridge diode, there is no significant loss in the resulting output voltage, and the rectified output effectively combines the TENG and PENG outputs. To demonstrate the potential application of the HTPENG devices, three capacitors with different capacitance values have been charged. Figure 5(c) shows the circuit diagram of the HTPENG for charging the capacitor. As shown in Fig. 5(d), we found that 1 μF capacitor can be charged to 2.5 V by the HTPENG within 80 s, while 3.3 and 10 μF capacitors can be charged to 1.0 and 0.25 V within 80 s, respectively. Figure 5(e) shows that the rectified HTPENG can directly drive three LED bulbs without any storage unit. Therefore, when we enlarge the surface area of the HTPENG to obtain more output, we can use it as a powerful mechanical

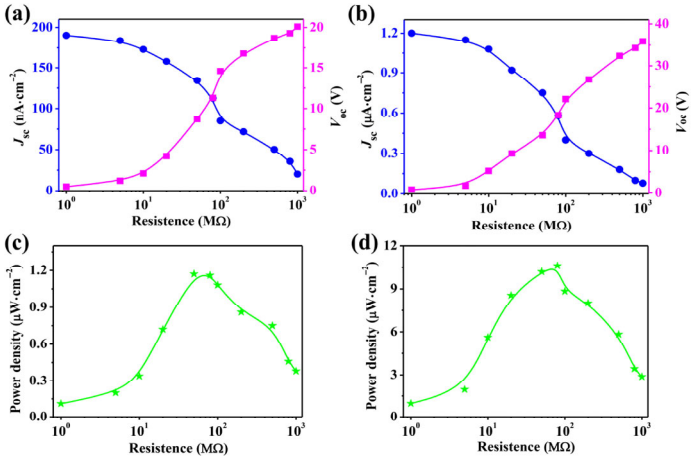

Figure 4 The output power of the triboelectric part and the piezoelectric part. (a) The short-circuit current density and open-circuit voltage of the piezoelectric part under the varied external load resistances. (b) The short-circuit current density and open-circuit voltage of the triboelectric part under varied external load resistances. (c) The power density of the piezoelectric part. (d) The power density of the triboelectric part.

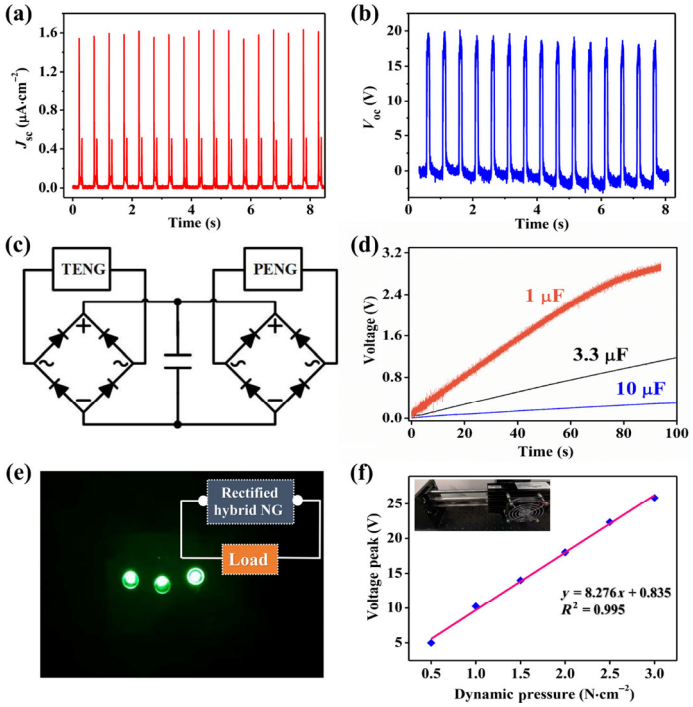

Figure 5 The HTPENG of output and related applications. (a) Short-circuit output current density of the HTPENG. (b) The open-circuit output voltage of the HTPENG. (c) Circuit diagram of the HTPENG for charging the capacitor. (d) Three capacitors of different capacitance values. (e) LEDs lit by the rectified HTPENG, the inset shows a schematic diagram of the connection circuit. (f) Relationship of output voltage peak of HTPENG and the dynamic pressure.

energy harvesting unit. In addition, the flexible HTPENG can also function as a pressure sensor that could output electrical signals without external power supply. Figure 5(f) shows the influence of contact-separation dynamic pressure on the performance of the HTPENG. It can be observed that the output peak voltage increases with the increase of the dynamic pressure. There is a linear relationship between the output voltage peak and the input dynamic pressure. The linear range of the dynamic pressure is from to 3 N·cm^{-2} with a high sensitivity of 8.276 V·cm^2·N^{-1} and a detection limit of 0.2 N·cm^{-2}.

4 Conclusions

In summary, we demonstrate the novel HTPENG with a simple, prototypical structure using functionalized BC paper and Nitro-CNF paper. Both triboelectric paper and piezoelectric paper with an area of 1.5 cm × 1.0 cm are produced by vacuum filtration without the additional surface modification. With the 5 Hz and 2 N·cm^{-2}, periodic varied external force in the open-circuit, the PENG and TENG output peak voltages are 22 and 37 V. And in the short-circuit, the PENG and TENG output peak current density are 220 nA·cm^{-2} and 1.23 μA·cm^{-2}. The piezoelectric output power density is 1.21 μW·cm^{-2} under the matched resistance of 60 MΩ, and the triboelectric output power density is 10.6 μW·cm^{-2} under the matched resistance of 80 MΩ. After rectification by a full wave bridge diode, the open-circuit voltage and the short-circuit current density of the HTPENG are 18 V and 1.6 μA·cm^{-2}, respectively. The rectified output power is enough to light three LED bulbs and charge a 1 μF capacitor to 2.5 V in the 80 s. In addition, the linear correlation pulse voltage signal generated by the HTPENG in contact-separation mode can be used for dynamic pressure detection. The linear range of dynamic pressure is from 0.5 to 3 N·cm^{-2} with a high sensitivity of 8.276 V·cm^2·N^{-1} and a detection limit of 0.2 N·cm^{-2}. The green and lightweight HTPENG can open up a new path for the design and application of hybrid nanogenerators with high flexibility and simple structure.

Acknowledgements

We thank the financial support from the Beijing Municipal Science & Technology Commission, China (Nos. Z171100002017017 and Z181100008818081), the National Key R & D Project from Minister of Science and Technology, China (No. 2016YFA0202702), the National Natural Science Foundation of China (Nos. 51873020, 21575009, 51432005, and Y4YR011001), the "Thousands Talents" program for pioneer researcher and his innovation team, China, the National Postdoctoral Program for Innovative Talents (No. BX20180081), and China Postdoctoral Science Foundation (No. 2019M650604).

References

[1] Liu, L.; Tang, W.; Deng, C. R.; Chen, B. D.; Han, K.; Zhong, W.; Wang, Z. L. Self-powered versatile shoes based on hybrid nanogenerators. *Nano Res*. **2018**, *11*, 3972–3978.

[2] Sun, C. L.; Shi, J.; Bayerl, D. J.; Wang, X. D. PVDF microbelts for harvesting energy from respiration. *Energy Environ*. *Sci*. **2011**, *4*, 4508–4512.

[3] Yang, J.; Chen, J.; Liu, Y.; Yang, W. Q.; Su, Y. J.; Wang, Z. L. Triboelectrification-based organic film nanogenerator for acoustic energy harvesting and self-powered active acoustic sensing. *ACS Nano* **2014**, *8*, 2649–2657.

[4] Pan, L.; Wang, J. Y.; Wang, P. H.; Gao, R. J.; Wang, Y. C.; Zhang, X. W.; Zou, J. J.; Wang, Z. L. Liquid-FEP-based U-tube triboelectric nanogenerator for harvesting water-wave energy. *Nano Res*. **2018**, *11*, 4062–4073.

[5] Wang, Z. L.; Song, J. H. Piezoelectric nanogenerators based on zinc oxide nanowire arrays. *Science* **2006**, *312*, 242–246.

[6] Jenkins, K.; Kelly, S.; Nguyen, V.; Wu, Y.; Yang, R. S. Piezoelectric diphenylalanine peptide for greatly improved flexible nanogenerators. *Nano Energy* **2018**, *51*, 317–323.

[7] Guo, H. Y.; Chen, J.; Tian, L.; Leng, Q.; Xi, Y.; Hu, C. G. Airflow-induced triboelectric nanogenerator as a self-powered sensor for detecting humidity and airflow rate. *ACS Appl*. *Mater*. *Interfaces* **2014**, *6*, 17184–17189.

[8] Han, C. B.; Zhang, C.; Tang, W.; Li, X. H.; Wang, Z. L. High power triboelectric nanogenerator based on printed circuit board (PCB) technology. *Nano Res*. **2015**, *8*, 722–730.

[9] Soin, N.; Zhao, P. F.; Prashanthi, K.; Chen, J. K.; Ding, P.; Zhou, E. P.; Shah, T.; Ray, S. C.; Tsonos, C.; Thundat, T. et al. High performance triboelectric nanogenerators based on phase-inversion piezoelectric membranes of poly(vinylidene fluoride)-zinc stannate (PVDF-$ZnSnO_3$) and polyamide-6 (PA6). *Nano Energy* **2016**, *30*, 470–480.

[10] Zhu, G.; Chen, J.; Liu, Y.; Bai, P.; Zhou, Y. S.; Jing, Q. S.; Pan, C. F.; Wang, Z. L. Linear-grating triboelectric generator based on sliding electrification. *Nano Lett*. **2013**, *13*, 2282–2289.

[11] Yuan, Z. Q.; Zhou, T.; Yin, Y. Y.; Cao, R.; Li, C. J.; Wang, Z. L. Transparent and flexible triboelectric sensing array for touch security applications. *ACS Nano* **2017**, *11*, 8364–8369.

[12] Zhu, G.; Yang, R. S.; Wang, S. H.; Wang, Z. L. Flexible high-output nanogenerator based on lateral ZnO nanowire array. *Nano Lett*. **2010**, *10*, 3151–3155.

[13] Zhang, L. M.; Han, C. B.; Jiang, T.; Zhou, T.; Li, X. H.; Zhang, C.; Wang, Z. L. Multilayer wavy-structured robust triboelectric nanogenerator for harvesting water wave energy. *Nano Energy* **2016**, *22*, 87–94.

[14] Pang, Y. K.; Li, X. H.; Chen, M. X.; Han, C. B.; Zhang, C.; Wang, Z. L. Triboelectric nanogenerators as a self-powered 3D acceleration sensor. *ACS Appl*. *Mater*. *Interfaces* **2015**, *7*, 19076–19082.

[15] Dhakar, L.; Tay, F. E. H.; Lee, C. Investigation of contact electrification based broadband energy harvesting mechanism using elastic PDMS microstructures. *J*. *Micromech*. *Microeng*. **2014**, *24*, 104002.

[16] Zhang, X. S.; Han, M. D.; Wang, R. X.; Zhu, F. Y.; Li, Z. H.; Wang, W.; Zhang, H. X. Frequency-multiplication high-output triboelectric nanogenerator for sustainably powering biomedical microsystems. *Nano Lett*. **2013**, *13*, 1168–1172.

[17] Xu, X.; Potié, A.; Songmuang, R.; Lee, J. W.; Bercu, B.; Baron, T.; Salem, B.; Montès, L. An improved AFM cross-sectional method for piezoelectric nanostructures properties investigation: Application to GaN nanowires. *Nanotechnology* **2011**, *22*, 105704.

[18] Chang, C.; Tran, V. H.; Wang, J. B.; Fuh, Y. K.; Lin, L. W. Direct-write piezoelectric polymeric nanogenerator with high energy conversion efficiency. *Nano Lett*. **2010**, *10*, 726–731.

[19] Park, K. I.; Lee, M.; Liu, Y.; Moon, S.; Hwang, G. T.; Zhu, G.; Kim, J. E.; Kim, S. O.; Kim, D. K.; Wang, Z., L. et al. Flexible nanocomposite generator made of $BaTiO_3$ nanoparticles and graphitic carbons. *Adv*. *Mater*. **2012**, *24*, 2999–3004.

[20] Yang, Y.; Guo, W. X.; Pradel, K. C.; Zhu, G.; Zhou, Y. S.; Zhang, Y.; Hu, Y. F.; Lin, L.; Wang, Z. L. Pyroelectric nanogenerators for harvesting thermoelectric energy. *Nano Lett.* **2012**, *12*, 2833–2838.

[21] Tao, K.; Hu, W.; Xue, B.; Chovan, D.; Brown, N.; Shimon, L. J. W.; Maraba, O.; Cao, Y.; Tofail, S. A. M.; Thompson, D. et al. Bioinspired stable and photoluminescent assemblies for power generation. *Adv*. *Mater*. **2019**, *31*, 1807481.

[22] Yuan, H.; Lei, T. M.; Qin, Y.; Yang, R. S. Flexible electronic skins based on piezoelectric nanogenerators and piezotronics. *Nano Energy* **2019**, *59*, 84–90.

[23] Yuan, H.; Lei, T. M.; Qin, Y.; He, J. H.; Yang, R. S. Design and application of piezoelectric biomaterials. *J*. *Phys*. *D*: *Appl*. *Phys*. **2019**, *52*, 194002.

[24] Liu, S. L.; Tao, D. D.; Bai, H. Y.; Liu, X. Y. Cellulose-nanowhisker-templated synthesis of titanium dioxide/cellulose nanomaterials with promising photocatalytic abilities. *J*. *Appl*. *Polym*. *Sci*. **2012**, *126*, E282–E290.

[25] Zeng, J.; Li, R.; Liu, S. L.; Zhang, L. N. Fiber-like TiO_2 nanomaterials with different crystallinity phases fabricated via a green pathway. *ACS Appl*. *Mater*. *Interfaces* **2011**, *3*, 2074–2079.

[26] Moon, R. J.; Martini, A.; Nairn, J.; Simonsen, J.; Youngblood, J. Cellulose nanomaterials review: Structure, properties and nanocomposites. *Chem*. *Soc*. *Rev*. **2011**, *40*, 3941–3994.

[27] Zhou, Y. H.; Khan, T. M.; Liu, J. C.; Fuentes-Hernandez, C.; Shim, J. W.; Najafabadi, E.; Youngblood, J. P.; Moon, R. J.; Kippelen, B. Efficient recyclable organic solar cells on cellulose nanocrystal substrates with a conducting polymer top electrode deposited by film-transfer lamination. *Org*. *Electron*. **2014**, *15*, 661–666.

[28] Yao, C. H.; Hernandez, A.; Yu, Y. H.; Cai, Z. Y.; Wang, X. D. Triboelectric nanogenerators and power-boards from cellulose nanofibrils and recycled materials. *Nano Energy* **2016**, *30*, 103–108.

[29] Zhang, L. C.; Sun, X.; Hu, Z.; Yuan, C. C.; Chen, C. H. Rice paper as a separator membrane in lithium-ion batteries. *J*. *Power Sources* **2012**, *204*, 149–154.

[30] Yao, C. H.; Yin, X.; Yu, Y. H.; Cai, Z. Y.; Wang, X. D. Chemically functionalized natural cellulose materials for effective triboelectric nanogenerator development. *Adv*. *Funct*. *Mater*. **2017**, *27*: 1700794.

[31] Zhang, G. J.; Liao, Q. L.; Zhang, Z.; Liang, Q. J.; Zhao, Y. L.; Zheng, X.; Zhang, Y. Novel piezoelectric paper-based flexible nanogenerators composed of $BaTiO_3$ nanoparticles and bacterial cellulose. *Adv*. *Sci*. **2016**, *3*, 1500257